









Cite this: *Environ. Sci.: Water Res. Technol.*, 2024, **10**, 2142

## Efficient and effective removal of toluene from aqueous solution using MIL-100(Fe)<sup>†</sup>

Catalina V. Flores, <sup>ab</sup> Juan L. Obeso, <sup>ab</sup> Herlys Viltres, <sup>c</sup>  
Ricardo A. Peralta, <sup>\*d</sup> Ilich A. Ibarra <sup>\*be</sup> and Carolina Leyva <sup>\*a</sup>

The MIL-100(Fe) was employed for the remediation of toluene-contaminated water. The MIL-100(Fe) samples synthesised for this work exhibit high thermal (300 °C) and chemical (pH range 2–10) stability. Adsorption kinetics and isotherms were fitted to the Elovich and Temkin models. The pH of the aqueous sample containing Toluene impacted the adsorption capacity of MIL-100(Fe) through modulation of the MOF  $\zeta$  potential. As a result, we concluded that MIL-100(Fe) is most effective at adsorbing toluene in the 6–10 pH range, a finding that underscores its potential in water treatment. The maximum Langmuir adsorption capacity of 318.48 mg g<sup>-1</sup> was determined. MIL-100(Fe) showed excellent adsorption-desorption performance and stability; hence, it can be used repeatedly without losing toluene adsorption capacity. FT-IR spectra suggest that  $\pi$ - $\pi$  interactions serve a crucial role during toluene adsorption, further confirming the effectiveness of MIL-100 (Fe) in water treatment.

Received 15th June 2024,  
Accepted 4th July 2024

DOI: 10.1039/d4ew00503a

rsc.li/es-water

### Water impact

Due to the lack of research focused on removing VOCs from aqueous solutions, this study presents the application of MIL-100(Fe), an advanced adsorbent, for toluene removal from water, an aromatic VOC of high toxicity. MIL-100(Fe) is a promising system for VOC adsorption and illustrates how these systems need to be further explored in applications that impact our environment.

## Introduction

Water pollution, a pressing environmental issue that arises from the uncontrolled release of wastewater from the vast industrial and municipal sectors,<sup>1</sup> has escalated due to the burgeoning human population. This pollution has a profound impact on aquatic ecosystems. Generally, the main pollutants are organic dyes, heavy metals, nutrients, pharmaceuticals, and volatile organic compounds (VOCs).<sup>2</sup>

Furthermore, VOCs are chemical complexes based on aromatic and hydrocarbon structures.<sup>2</sup> VOCs are highly persistent in the environment and are classified as harmful and toxic pollutants. VOCs participate in atmospheric photochemical reactions that promote ozone formation,<sup>3</sup> due to their usually being found in the vapor phase. However, VOCs can be located in soil<sup>4</sup> and water<sup>5</sup> mainly due to anthropogenic activities, such as refineries,<sup>6</sup> pharmaceuticals<sup>7</sup> and textiles manufacturers,<sup>8</sup> and natural (biogenic) sources.<sup>9</sup> In this context, the presence of VOCs pollutants in water ecosystems has emerged as a problem. The main concern is the lack of monitoring of VOCs in water systems. The family of VOC aromatics (benzene, toluene, and xylenes) are the most persistent in water.<sup>10</sup> Specifically, toluene is a widely known raw material for diverse solvents, inks, and adhesives applications.<sup>11</sup> Toluene molecules have displayed high toxicity for human health, even at low concentrations.<sup>12</sup>

Thus, developing methodologies to remove toluene from the water matrix is necessary. Adsorbents such as zeolites<sup>13</sup> and activated carbon<sup>14</sup> have been employed to remove VOCs from water, but they have been demonstrated to be ineffective. As an alternative, Metal-Organic Frameworks (MOFs) are crystal materials formed of metal ion centers

<sup>a</sup> Instituto Politécnico Nacional, CICATA U. Legaria, Laboratorio Nacional de Ciencia, Tecnología y Gestión Integrada del Agua (LNAgua), Legaria 694, Col. Irrigación, Miguel Hidalgo, 11500, CDMX, Mexico. E-mail: zleyva@ipn.mx

<sup>b</sup> Laboratorio de Físicoquímica y Reactividad de Superficies (LaFREs), Instituto de Investigaciones en Materiales, Universidad Nacional Autónoma de México, Circuito Exterior s/n, CU, Coyoacán, 04510, Ciudad de México, Mexico. E-mail: argel@unam.mx

<sup>c</sup> School of Engineering Practice and Technology, McMaster University, 1280 Main Street West Hamilton, ON, L8S 4L8, Canada

<sup>d</sup> Departamento de Química, División de Ciencias Básicas e Ingeniería, Universidad Autónoma Metropolitana (UAM-I), 09340, Mexico. E-mail: rperalta@izt.uam.mx

<sup>e</sup> On sabbatical as “Catedra Dr. Douglas Hugh Everett” at Departamento de Química, Universidad Autónoma Metropolitana-Iztapalapa, Avenida San Rafael Atlixco 186, Leyes de Reforma 1ra Sección, Iztapalapa, 09310 Ciudad de México, Mexico

<sup>†</sup> Electronic supplementary information (ESI) available: Instrumental techniques, characterization, and computational chemistry. See DOI: <https://doi.org/10.1039/d4ew00503a>



linked by organic ligands.<sup>15</sup> They are highly porous and structurally stable, making them excellent adsorbents for removing pollutants from water.

Different MOF materials have been applied to remediate toluene in the gas phase. UiO-66-NH<sub>2</sub>, UiO-66, MOF-199, and ZIF-67 show high adsorption capacity involving hydrogen bonding and  $\pi$ - $\pi$  complexation as the main interactions.<sup>16</sup> Based on this outstanding result of applying MOF materials for toluene adsorption, the evaluation of MOF in aqueous media is analyzed. Furthermore, the implementation of iron-containing MOFs, such as MIL-100(Fe), is desirable for water remediation due to their low cost, high stability in water, high porosity compared to conventional adsorbents, excellent performance, reusability, and low toxicity (compared to chromium, cobalt, and cadmium analogues), as well as their excellent performance in removing contaminants.

Thus, this study explores the application of an MOF material in the adsorption process for removing toluene from an aqueous solution using a Fe-based MOF. MIL-100(Fe) was characterized by different analytical techniques such as powder X-ray diffraction (PXRD), fourier-transform infrared spectroscopy (FTIR), thermogravimetric analysis (TGA), N<sub>2</sub> adsorption, scanning electron microscope (SEM), and X-ray photoelectron spectroscopy (XPS). The toluene quantification was performed using gas chromatography (GC) combined with an appropriate sample pretreatment. The effect of dosage, pH, contact time, concentration, selectivity, and reusability was studied. The main adsorption mechanism was determined by FTIR and XPS techniques. Hence, this research corroborates the prospective application of MOF materials for toluene remediation in water.

## Experimental

### Chemicals

Iron(III) chloride hexahydrate (FeCl<sub>3</sub>·6H<sub>2</sub>O, ≥98%), benzene-1,3,5-tricarboxylic acid (H<sub>3</sub>BTC, 95%), toluene (C<sub>6</sub>H<sub>5</sub>CH<sub>3</sub>, 99.5%), benzene (C<sub>6</sub>H<sub>6</sub>, 99.8%), xylene (C<sub>6</sub>H<sub>4</sub>(CH<sub>3</sub>)<sub>2</sub>, 98%), chlorobenzene (C<sub>6</sub>H<sub>5</sub>Cl, 99.8%), methanol (CH<sub>3</sub>OH, 99.8%), ethanol (CH<sub>3</sub>CH<sub>2</sub>OH, 95%), acetone (CH<sub>3</sub>COCH<sub>3</sub>, 99.5%), *n*-hexane (CH<sub>3</sub>(CH<sub>2</sub>)<sub>4</sub>CH<sub>3</sub>, 99.8%), nitric acid (HNO<sub>3</sub>, 70%), sodium hydroxide pellets (NaOH, 97%), anhydrous magnesium sulfate (MgSO<sub>4</sub>, 97%) and hydrofluoric acid (HF, 48%) were supplied by Sigma-Aldrich. High-purity deionized water with a specific resistance of 18.2 mΩ cm<sup>-1</sup> was obtained from a Mili-Q system Simplicity®. All reagents and solvents were used as received from commercial suppliers without further purification.

### Synthesis of MIL-100(Fe)

MIL-100(Fe) synthesis (Fig. S1†) was performed as reported by Guo and collaborators.<sup>17</sup> H<sub>3</sub>BTC linker (0.656 g, 3.94 mmol) and FeCl<sub>3</sub>·6H<sub>2</sub>O (0.972 g, 3.6 mmol) were dissolved in deionized water (20 mL) with HF (150 μL, 8.62 mmol) modulator. The mixed solution was transferred to a Teflon liner placed in an autoclave (50 mL), then heated to 150 °C

for 24 h. Subsequently, the powder was centrifugated and washed with water, ethanol, and acetone (three times) and dried at 100 °C overnight.

### Instruments

Detailed information on the instrumental techniques is available in section S1.†

### Adsorption experiments

Experiments were carried out in triplicates. Toluene adsorption evaluations were performed by adding a known mass (1–30 mg) of MIL-100(Fe) in a fixed volume (20 mL) with a toluene initial concentration (5–150 mg L<sup>-1</sup>) under stirring at a specific time (1440 min), at room temperature, under a controlled pH (2–10), at the end of the experiments through gas chromatography was analysed the residual amount of toluene by liquid–liquid extraction. More detailed information is available in the S2† section.

## Results and discussion

### Characterization of MIL-100(Fe)

On account of the promising characteristic of MIL-100(Fe) for aqueous remediation applications, we prepared samples of this MOF as per the previously reported synthesis by Simon *et al.*<sup>18</sup> The Powder X-ray Diffraction (PXRD) pattern obtained from our MIL-100(Fe) sample is similar to the simulated pattern (Fig. 1a) and previously reported data. Then, the Fourier Transform Infra-Red (FT-IR) spectrum (Fig. 1b) possesses the characteristic bands expected for MIL-100(Fe). The band at 484 cm<sup>-1</sup> corresponds to the Fe–O vibration, while the bands at 713, 758, 1383, and 1448 cm<sup>-1</sup> are related to the C–H stretching signals from the aromatic ring and the symmetric and asymmetric stretching vibrations of the carboxylate from the BTC ligand, respectively. Moreover, the band at 1576 cm<sup>-1</sup> indicates the vibration generated from C=C aromatics groups. The coordination of the C=O carbonyl group with the metal center is shown at the band at 1631 cm<sup>-1</sup>. Finally, the band at 3482 cm<sup>-1</sup> corresponds to the stretching of the –OH group. These bands agree with those reported previously for this material.<sup>19,20</sup> Further, the pH stability test conducted in the 2–10 interval indicates that MIL-100(Fe) retains its characteristic signals and bands as identified through FT-IR and PXRD analysis, without any modification in this interval.

The thermogravimetric analysis (TGA) (Fig. S2a†) shows thermal stability up to 300 °C. The weight loss is divided into three stages.<sup>21,22</sup> The first is related to moisture release. The second stage is associated with the breakdown of the MOF, with the decomposition of the unreacted H<sub>3</sub>BTC molecules, forming and detaching CO<sub>2</sub> from organic molecules' carbonization. And a third stage, above 550 °C, in which the structure collapses, forming residual Fe<sub>2</sub>O<sub>3</sub>.

The surface morphology of the MIL-100(Fe) obtained was analysed by SEM (Fig. S3a†). Particles of irregular superficial



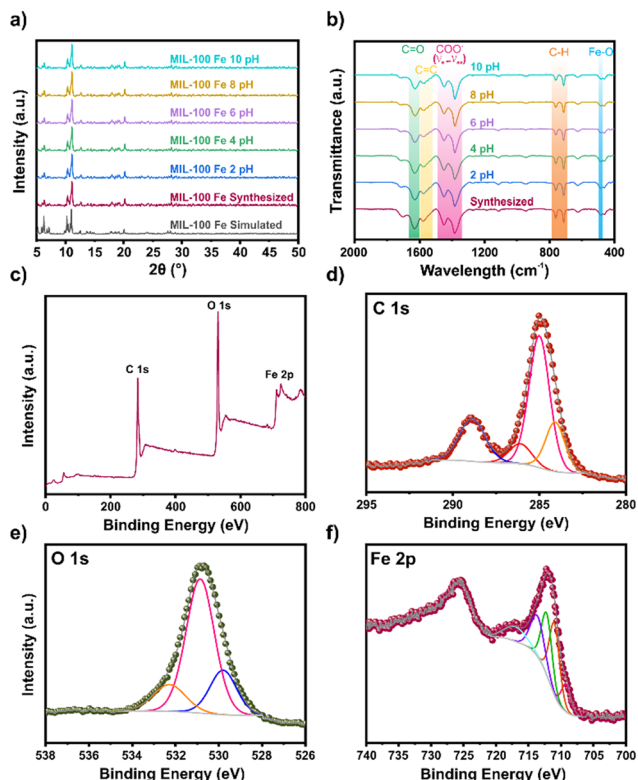


Fig. 1 a) PXRD pattern; b) FT-IR spectrum; c) XPS survey spectrum; high-resolution spectra of d) C 1s; e) O 1s; and f) Fe 2p of synthesized MIL-100(Fe).

morphology were obtained.<sup>23</sup> The surface element distribution analysis was also performed (Fig. S3b†). A homogeneous distribution of carbon, oxygen, and iron distribution was observed on the surface. The nitrogen adsorption measurements were performed at 77 K (Fig. S2b†). The isotherm obtained is similar to those reported previously for this material.<sup>24</sup> The calculated BET surface area was  $743 \text{ m}^2 \text{ g}^{-1}$ , with a volume pore of  $0.750 \text{ cm}^3 \text{ g}^{-1}$ . This surface area was similar to that reported by Nehra and collaborators.<sup>25</sup> X-ray photoelectron spectroscopy (XPS) analysis (Fig. 1c–f) was performed to obtain details of the chemical environment. The results of the survey spectra (Table S1†) corroborated C, O, and Fe presence in MIL-100(Fe). The high-resolution XPS spectra of C 1s (Fig. 1d) fit show peaks at 284.1, 285.0, 286.1, and 288.9 eV, attributed to the aromatic C=C of the linker, C-C/C-H, C-O due to OH groups, and -C=O for the carboxylic moieties,<sup>26</sup> respectively (Table S2†). The O 1s high-resolution (Fig. 1e) signals fit showed peaks at 529.8, 530.9, and 532.3 eV, related to Fe-O, C=O, and O-chemisorbed,<sup>27</sup> respectively (Table S3†). The Fe 2p high-resolution signals (Fig. 1f) fit showed peaks at 709.2, 711.0, 712.2, 713.6, and 717.0 eV, related to  $\text{Fe}^{+2}$ , and three different  $\text{Fe}^{+3}$  contributions, and satellite  $\text{Fe}^{+3}$  respectively (Table S4†).<sup>28</sup>

### Effect of parameters on toluene adsorption

Having thoroughly characterised the chemical and physical properties of MIL-100(Fe), we turned our attention towards

assessing the toluene adsorption performance of the material. Gas chromatography analysis was carried out to measure the amount of residual toluene. The sample was subjected to liquid-liquid extraction pretreatment to obtain an accurate analysis, which included preconcentration and isolation steps. The extraction process utilized *n*-hexane as the organic phase, chlorobenzene as the internal standard, and saturated magnesium sulphate as a dry agent. More detailed information can be found in section S2.†

This study investigated several factors that affect the adsorption of toluene by MIL-100(Fe). The impact of the amount of adsorbent dose used was examined by adding 1–30 mg of MIL-100(Fe) (Fig. 2a). It can be noticed an adsorption capacity decreases when the mass of the adsorbent increases. However, an increment of removal efficiency was observed from 57% to 80% from 1 to 30 mg, respectively (Fig. S6†). This can be attributed to the interaction sites increment as the mass increases.

We next considered the effect of pH on adsorption behaviour. The results reveal reduced adsorption capacity at pH 2–4 (Fig. 2b). Based on the  $\zeta$  potential analysis, we could attribute this behaviour to the agglomeration of particles close to the MIL-100(Fe) isoelectric point (pH 3.2), thereby reducing the adsorbent-adsorbate interaction. When the  $\zeta$  potential ranges between  $-30$  to  $+30$  mV, the particles tend to

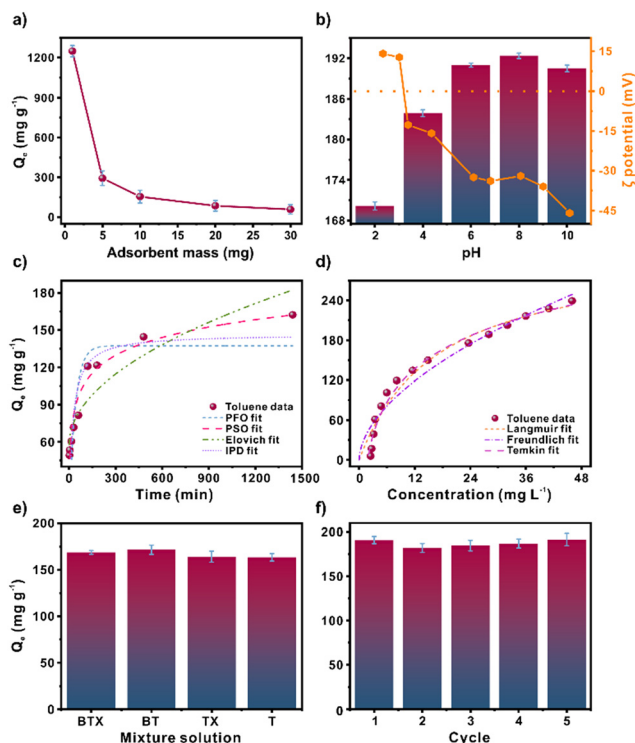


Fig. 2 a) Adsorbent mass effect [1–30 mg, 20 mL,  $100 \text{ mg L}^{-1}$ , 6.5 pH, 24 h]; b) pH solution effect [10 mg, 20 mL,  $100 \text{ mg L}^{-1}$ , 2–10 pH, 24 h]; c) kinetic fits [10 mg, 20 mL,  $100 \text{ mg L}^{-1}$ , 6.5 pH, 24 h]; d) isotherms fits [10 mg, 20 mL, 5–150  $\text{mg L}^{-1}$ , 6.5 pH, 24 h]; e) toluene (T) adsorption in presence of benzene (B) and xylene (X) [10 mg, 20 mL,  $100 \text{ mg L}^{-1}$ , 6.5 pH, 24 h]; and f) toluene adsorption in regenerated MIL-100(Fe) [10 mg, 20 mL,  $100 \text{ mg L}^{-1}$ , 6.5 pH, 24 h].





agglomerate and become less stable in dispersion.<sup>29</sup> Above pH 6, the  $\zeta$  potential is above  $-30$  mV. Thus, the entire surface area and interaction sites are exposed and available. The ideal pH operates in ranges of 6–10, in which the MIL-100(Fe) particles are dispersed in the solution. The variation in adsorption capacity is negligible, with a maximum adsorption capacity of  $192.36 \text{ mg g}^{-1}$  at pH 8 and a minimum adsorption capacity of  $190.47 \text{ mg g}^{-1}$  at pH 10.

### Adsorption kinetics and adsorption isotherms

Furthermore, non-linear fitting to the pseudo-first-order (PFO), pseudo-second-order (PSO), Elovich, and Intra-particle diffusion (IPD) kinetic models were analysed to study the adsorption kinetics of toluene over MIL-100(Fe) (Fig. 2c). The main parameters for each model are listed in Table S7†. The Elovich model displayed the best fit with a correlation coefficient ( $R^2$ ) of 0.950. This model often considers a slow adsorption rate based on chemical adsorption. Conversely, in an effort to better understand the interactions between MIL-100(Fe) and toluene molecules, a non-linear fitting of the Freundlich, Langmuir, and Temkin models was performed (Fig. 2d and Table S9). The fitting order concerning the correlation coefficient,  $R^2$ , was Temkin > Langmuir > Freundlich with values of 0.982, 0.963, and 0.937  $R^2$ , respectively. The Temkin model considers the indirect adsorbate–adsorbent interaction due to the heat of adsorption decreasing linearly with increasing adsorbent surface coverage.<sup>30</sup> It assumes a uniform distribution of interaction sites, similar to the Langmuir model.<sup>31</sup> The maximum adsorption capacity obtained was  $318.48 \text{ mg g}^{-1}$ . Compared to other reported toluene adsorbents (Table S5†), the material is highly competitive.

### Effect of coexistence pollutants and reusability

The ability of MIL-100(Fe) to adsorb toluene in the presence of other pollutants, such as benzene and a mixture of xylenes, was evaluated (Fig. 2e). Three experiments were conducted to assess the impact of these pollutants on toluene adsorption. The first experiment involved exposing MIL-100(Fe) to a mixture of benzene, toluene, and xylenes, while the second and third experiments involved a mixture of benzene and toluene, and xylenes, respectively. The results showed a negligible variation in the toluene adsorption capacity compared to the toluene adsorption alone. Hence, xylenes and benzene have minimal impact on toluene adsorption.

The ability to regenerate an adsorbent is highly beneficial since it increases the lifetime adsorption capacity of the adsorbent. Five toluene adsorption–desorption cycles were performed using MIL-100(Fe) to assess the reusability of the material (Fig. 2f). Due to the high boiling temperature of toluene ( $110^\circ\text{C}$ ), the desorption was performed at an elevated temperature of  $110^\circ\text{C}$  to ensure that adsorbed toluene was fully released from MIL-100(Fe). Across the adsorption–desorption cycles, negligible adsorption capacity

variation was noted. The structural stability of MIL-100(Fe) over the course of multiple adsorption–desorption cycles was evaluated (Fig. S5†) by PXRD analysis, which confirmed that the MIL-100(Fe) structure was preserved.

### Adsorption mechanism

To investigate the possible adsorption mechanism, we turned our attention to FT-IR spectroscopy of MIL-100(Fe) samples before and after toluene adsorption (Fig. 3a). The appearance of new bands at  $1045$  and  $1090 \text{ cm}^{-1}$  is attributed to C–H bending in the plane, and a variation in  $760 \text{ cm}^{-1}$  corresponds to C–H bending out of a plane from toluene.<sup>31,32</sup> Additionally, the appearance of a shoulder around  $1320 \text{ cm}^{-1}$  assigned to the C–C originated from the toluene aromatic ring adsorption in MIL-100(Fe).<sup>33</sup> The above and the changes in the FT-IR spectrum in the region related to the C=C and C=O stretching vibration from the aromatic ring and carboxyl groups may suggest a  $\pi$ – $\pi$  interaction among the aromatic toluene ring and the MIL-100(Fe).<sup>34</sup>

In order to analyse the adsorption mechanism within MIL-100(Fe), XPS analysis was performed. The high-resolution XPS spectra of C 1s fit before and after toluene adsorption show unaltered peaks (Fig. 3b). However, the high-resolution XPS spectra of O 1s (Fig. 3c) display slight shifts ( $0.1 \text{ eV}$ ) from the Fe–O and  $\text{C}=\text{O}$  peaks. This change was at lower energies from  $529.8$  to  $529.7 \text{ eV}$  and  $530.9$  to  $530.8 \text{ eV}$ , respectively. Similarly, the high-resolution XPS spectra of Fe 2p (Fig. 3d) show a shift to lower binding energies after the toluene adsorption in the  $\text{Fe}^{3+}$  contributions, from  $711.0$ ,  $712.2$ , and  $713.6$  to  $710.7$ ,  $711.7$ , and  $713.1 \text{ eV}$ .

These changes could be related to the coordination of water molecules through the open metal sites of MIL-100(Fe) since the adsorption process was *via* an aqueous solution.<sup>35</sup> In this scenario, the toluene molecule could enter the MIL-

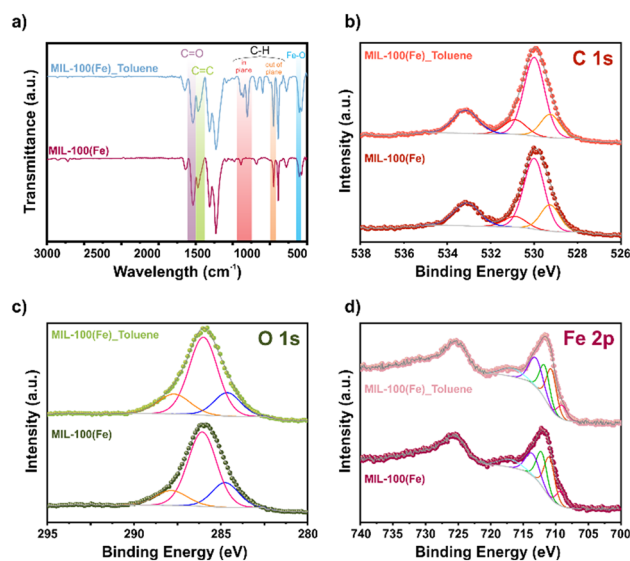


Fig. 3 a) FT-IR spectrum and high-resolution spectra of b) C 1s; c) O 1s; and d) Fe 2p for MIL-100(Fe).



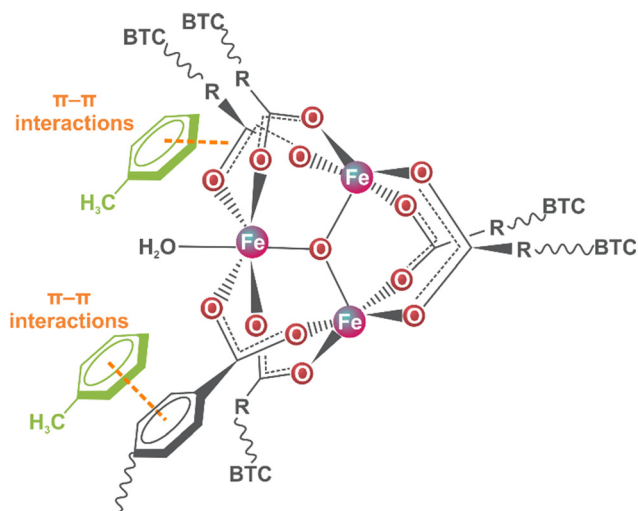


Fig. 4 Possible adsorption mechanism for toluene adsorption using MIL-100(Fe).

100(Fe) pore and interrelate *via*  $\pi$ - $\pi$  interaction with the organic linkers due to the low availability of the metal centre for water coordination.<sup>36</sup> The above analysis proposed the possible interaction mechanism (Fig. 4) between the toluene molecules and MIL-100(Fe).

## Conclusion

In summary, we have evaluated the effect of several relevant factors on the toluene adsorption behaviour of MIL-100(Fe), including kinetic models, adsorption isotherms, mass dosage, pH of the polluted sample, the presence of coexisting pollutants, adsorption-desorption cycles, and the characterization of MIL-100(Fe). The optimal pH range was determined to be pH 6–10 since the  $\zeta$  potential of MIL-100(Fe) at lower pH promotes agglomeration of the MIL-100(Fe) particles in the solution, which is detrimental to toluene adsorption capacity. The Langmuir maximum adsorption capacity was estimated to be 318.48 mg g<sup>-1</sup>, a highly competitive value considering the alternative adsorbents used for toluene adsorption. MIL-100(Fe) exhibits outstanding adsorption-desorption performance over multiple cycles. FT-IR and XPS characterizations suggest a  $\pi$ - $\pi$  interaction, along the C=C and C=O in MIL-100(Fe) with the toluene ring, as the possible adsorption mechanism. Overall, this work demonstrates that MIL-100(Fe) is a promising system for toluene adsorption and illustrates how these systems need to be further explored in applications that impact our environment.

## Data availability

All data is available in the main manuscript and ESI.†

## Conflicts of interest

There are no conflicts to declare.

## Acknowledgements

The authors thank U. Winnberg (Euro Health) for scientific discussions and G. Ibarra-Winnberg for scientific encouragement. C. V. F and J. L. O. thank CONAHCYT for the Ph.D. fellowships (1040318 and 1003953). C. L. thanks to the IPN projects (20241189 and 20242829).

## References

- 1 J. Mikosz, *Int. J. Environ. Sci. Technol.*, 2015, **12**, 827–836.
- 2 S. Madhav, A. Ahamad, A. K. Singh, J. Kushawaha, J. S. Chauhan, S. Sharma and P. Singh, in *Sensors in Water Pollutants Monitoring: Role of Material*, ed. D. Pooja, P. Kumar, P. Singh and S. Patil, Springer Singapore, Singapore, 2020, pp. 43–62.
- 3 Y. Zhang, T. Zang, B. Yan and C. Wei, *Int. J. Environ. Res. Public Health*, 2020, **17**, 553.
- 4 K. Schulz-Bohm, S. Geisen, E. R. J. Wubs, C. Song, W. De Boer and P. Garbeva, *ISME J.*, 2017, **11**, 817–820.
- 5 A. Nikolaou, *Water Res.*, 2002, **36**, 2883–2890.
- 6 S. Saikomol, S. Thepanondh and W. Laowagul, *J. Environ. Health Sci. Eng.*, 2019, **17**, 561–570.
- 7 V. S. Priya and L. Philip, *Chem. Eng. J.*, 2015, **266**, 309–319.
- 8 Z. Liang, J. Wang, Y. Zhang, C. Han, S. Ma, J. Chen, G. Li and T. An, *J. Cleaner Prod.*, 2020, **253**, 120019.
- 9 P. K. Padhy and C. K. Varshney, *Chemosphere*, 2005, **59**, 1643–1653.
- 10 C. Wang, W. Wang, S. Shao, W. Deng, C. Wang, X. Liu, H. Li, M. Wen, X. Zhang, G. Li and T. An, *Sci. Total Environ.*, 2024, **917**, 170407.
- 11 S. L. Cruz, M. T. Rivera-García and J. J. Woodward, *J. Drug Alcohol Res.*, 2014, **3**, 1–8.
- 12 M. Rooseboom, N. A. Kocabas, C. North, R. J. Radcliffe and L. Segal, *Regul. Toxicol. Pharmacol.*, 2023, **141**, 105387.
- 13 Z. Mamaghanifar, A. Heydarinasab, A. Ghadi and E. Binaeian, *Water Conserv. Sci. Eng.*, 2020, **5**, 1–13.
- 14 H. Anjum, K. Johari, N. Gnanasundaram, A. Appusamy and M. Thanabalan, *J. Mol. Liq.*, 2019, **280**, 238–251.
- 15 S. L. James, *Chem. Soc. Rev.*, 2003, **32**, 276.
- 16 K. Vellingiri, P. Kumar, A. Deep and K.-H. Kim, *Chem. Eng. J.*, 2017, **307**, 1116–1126.
- 17 X.-Z. Guo, S.-S. Han, J.-M. Yang, X.-M. Wang, S.-S. Chen and S. Quan, *Ind. Eng. Chem. Res.*, 2020, **59**, 2113–2122.
- 18 M. A. Simon, E. Anggraeni, F. E. Soetaredjo, S. P. Santoso, W. Irawaty, T. C. Thanh, S. B. Hartono, M. Yuliana and S. Ismajji, *Sci. Rep.*, 2019, **9**, 16907.
- 19 B. T. Le, D. D. La and P. T. H. Nguyen, *ACS Omega*, 2023, **8**, 1262–1270.
- 20 S. Rostamnia and H. Alamgholiloo, *Catal. Lett.*, 2018, **148**, 2918–2928.
- 21 S. Huang, K.-L. Yang, X.-F. Liu, H. Pan, H. Zhang and S. Yang, *RSC Adv.*, 2017, **7**, 5621–5627.



- 22 C. R. Quijia, C. Lima, C. Silva, R. C. Alves, R. Frem and M. Chorilli, *J. Drug Deliv. Sci. Technol.*, 2021, **61**, 102217.
- 23 W. Li, T. Zhang, L. Lv, Y. Chen, W. Tang and S. Tang, *Colloids Surf., A*, 2021, **624**, 126791.
- 24 M. Ahmad, S. Chen, F. Ye, X. Quan, S. Afzal, H. Yu and X. Zhao, *Appl. Catal., B*, 2019, **245**, 428–438.
- 25 M. Nehra, N. Dilbaghi, N. K. Singhal, A. A. Hassan, K.-H. Kim and S. Kumar, *Environ. Res.*, 2019, **169**, 229–236.
- 26 F. Zhang, J. Shi, Y. Jin, Y. Fu, Y. Zhong and W. Zhu, *Chem. Eng. J.*, 2015, **259**, 183–190.
- 27 J.-H. Kim, H.-Y. Jang, S.-B. Kim, J.-W. Choi and J.-A. Park, *Water, Air, Soil Pollut.*, 2022, **233**, 480.
- 28 Y. Meng, Y. Huang, G. Huang and Y. Song, *RSC Adv.*, 2023, **13**, 28148–28157.
- 29 A. Barhoum, M. L. García-Betancourt, H. Rahier and G. Van Assche, in *Emerging Applications of Nanoparticles and Architecture Nanostructures*, Elsevier, 2018, pp. 255–278.
- 30 N. Ayawei, A. N. Ebelegi and D. Wankasi, *J. Chem.*, 2017, **2017**, 1–11.
- 31 H. Wang, D. J. Grant, P. C. Burns and C. Na, *Langmuir*, 2015, **31**, 5820–5826.
- 32 L. Heredia, E. Colombo, P. Quaino and S. Collins, *Top. Catal.*, 2022, **65**, 934–943.
- 33 O. Baytar, Ö. Şahin, S. Horoz and S. Kutluay, *Environ. Sci. Pollut. Res.*, 2020, **27**, 26191–26210.
- 34 Y. Hou, Z. Li, S. Ren and W. Wu, *Fuel Process. Technol.*, 2015, **135**, 99–104.
- 35 S.-H. Huo and X.-P. Yan, *J. Mater. Chem.*, 2012, **22**, 7449.
- 36 X. Ma, W. Wang, C. Sun, H. Li, J. Sun and X. Liu, *Sci. Total Environ.*, 2021, **793**, 148622.

